Component Noise Modeling for Distributed Propulsion Blown-Flap STOL Vehicle Flight Procedures

Nathan Yeung, Victoria Pellerito, Jessica De la Cruz, and Melody Emmanouilidi *
University of California Irvine, 4200 Engineering Gateway, Irvine, CA, 92697

Jacqueline L. Huynh†
University of California Irvine, 4200 Engineering Gateway, Irvine, CA, 92697

This paper describes the development of a component-based noise modeling methodology to examine flight procedures and resulting community noise levels for distributed propulsion (DP), blown-flap Short Takeoff and Landing (STOL) aircraft for Advanced Air Mobility applications. DP blown-flap STOL aircraft are able to achieve short takeoff and landing field lengths and steep climb and descent profiles, which are shown in a demonstration flight test to have potentially lower overflight noise levels in comparison to conventional flight procedures. However, distributed propulsion and blown-flaps present unique sources of noise that must be modeled to assess the overall procedural noise levels. The present methodology assesses the impact of propeller wake velocity, thrust, and flap configuration, which govern the flight performance characteristics of these aircraft, on noise. These performance states, airframe geometries, and flight procedure parameters such as flight path angle and speed, are inputted into a noise modeling framework that incorporates methods from the NASA Aircraft NOise Prediction Program 2. Such a framework predicts engine and airframe component noise, emphasizing propeller noise and propeller wake influence on flaps. The modeling results when demonstrated on a sub-scale STOL aircraft indicate that propeller noise is dominant during departure and cruise, but propeller wake-flap interaction noise can be significant on approach procedures. Modeling results also indicate that DP STOL aircraft equipped with high-lift devices have wide operating conditions, leading to the potential to optimize flight procedures for noise attenuation.

I. Nomenclature

AAM	=	Advanced Air Mobility
$ANOPP$	=	Aircraft NOise Prediction Program
C_L	=	Coefficient of Lift
$CTOL$	=	Conventional Takeoff and Landing
D	=	Drag
dB	=	Decibels
DP	=	Distributed Propulsion
GPS	=	Global Positioning System
ft	=	Feet
$L_{A,Max}$	=	Maximum A-weighted Sound Pressure Level
m	=	Meters
R	=	Propeller Radius
RPM	=	Revolutions per Minute
SEL	=	Sound Exposure Level
SPL	=	Sound Pressure Level
$STOL$	=	Short Takeoff and Landing

*Graduate Student Researcher, Department of Mechanical and Aerospace Engineering at the University of California Irvine, 4200 Engineering Gateway, Irvine, CA 92697, and AIAA Student Member.

†Assistant Professor, Department of Mechanical and Aerospace Engineering at the University of California Irvine, 4200 Engineering Gateway, Irvine, CA, 92697, and AIAA Member

T	=	Thrust
V_∞	=	Aircraft Flight Velocity
V_J	=	Propeller Wake Velocity
$VTOL$	=	Vertical Takeoff and Landing
W	=	Weight
δ_f	=	Flap Deflection Angle
γ	=	Flight Path Angle
ρ	=	Atmospheric Density

II. Introduction

Advanced Air Mobility (AAM) has the potential to enhance air travel accessibility for a variety of markets. However, noise remains a major constraint for vehicles being proposed for AAM, particularly for aircraft that feature multiple open propellers that interact with each other and with other airframe components [1]. Noise modeling at both the component level and flight procedural level is one method used to examine noise mitigation solutions. Previous work indicates that in order to determine overall community noise impact, noise assessments must consider the combination of both flight procedures and noise components in various operating conditions [2, 3].

Various AAM aircraft configurations are being proposed by the industry, such as vertical takeoff and landing (VTOL) and short takeoff and landing (STOL) vehicles [4], the latter of which are the focus of this paper. STOL vehicles equipped with distributed propulsion (DP), blown-flap technology are capable of short field performance compared to conventional takeoff and landing procedures (CTOL). The blown-jet produced by propellers arranged along and under the wing's leading edge enhances lift through interaction with the trailing edge flaps [5]. The achievement of high lift coefficients with this concept was recently demonstrated through wind tunnel tests of a blown-wing section and flight tests of a sub-scale demonstrator vehicle [5, 6] built by researchers at the Massachusetts Institute of Technology (MIT). Various lift and drag coefficients, as well as takeoff and landing field lengths and flight path angles, can be achieved with varying combinations of propeller arrangements, flap deflection angles, propeller rotational speed (RPM), aircraft flight speed V_∞, and power requirements.

This work seeks to demonstrate the potential noise variation for different STOL flight procedures and DP, blown-flap component noise. This is done through the examination of both noise source and flight procedure characteristics for STOL vehicles in general and DP blown-flap STOL vehicles in particular. The component-based noise analysis methodology is developed to be capable of estimating the flight performance and resulting noise impacts of different operating states in approach and departure for DP, blown-flap STOL performance. The noise levels of such flight procedures are examined in part through a flight demonstration and noise measurement test of a Helio Courier aircraft performing STOL approach and departures in comparison to noise levels measured during the performance of CTOL flight procedures. In addition, the propeller noise modeling in this framework is demonstrated and validated against experimental noise data. Finally, the full modeling methodology is exercised through the noise analysis of representative flight procedures of the sub-scale STOL demonstrator built at MIT [6].

A. Source Noise Characteristics of DP Blown-flap STOL Vehicles

Source characteristics for distributed propulsion, blown-flap vehicles are technology that is likely to differ from conventional, fixed-wing propeller aircraft or other vertical takeoff and landing aircraft. Partially due to high speeds near the tip, open propeller aircraft generate high noise signatures in near-static conditions. In addition, the inclusion of multiple propellers, conceptually seen in Fig. 1, results in propeller-propeller interaction noise sources [1].

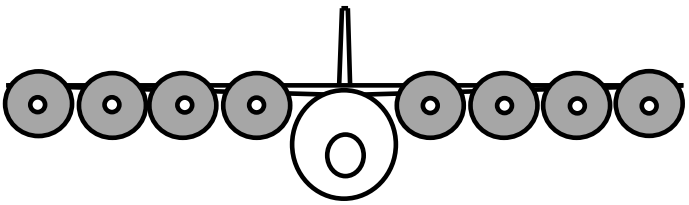

Fig. 1 Representative blown-flap STOL aircraft with distributed propulsors

In addition to propulsor sources, the propeller wake also interacts with the wing's trailing edge and flaps, as shown schematically in Fig. 2. For conventional aircraft, flap side edge noise is a significant airframe noise component, particularly during landing. This is due to the flow separation and vortex interactions near the side edge that scale according to the local flow velocity [7]. The jet produced by the propeller wake increases the flow velocity at the flap side edge and will increase wing trailing edge noise, as it is also a function of the local flow velocity [8]. This effect has been shown in previous noise measurements of blown-flap interaction noise to scale with approximately the 6^{th} power of the jet velocity [9]. Noise sources from other airframe components that are not a result of the propeller wake velocity, such as landing gear, can be expected to produce similar noise levels to those of conventional aircraft.

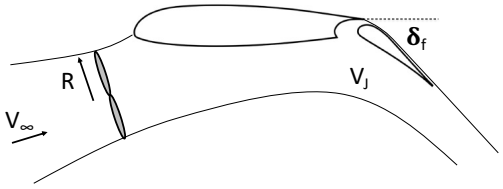

Fig. 2 Propeller wake interaction with the flap in blown-flap STOL aircraft

Assessment of the overall source noise levels of DP, blown-flap STOL vehicles requires consideration of the propeller tonal and broadband noise levels, airframe noise levels, and propeller wake-airframe interaction noise sources. These noise sources are influenced by performance attributes such as propeller arrangements, flap deflection, propeller rotation rate (RPM), aircraft speed, power requirements, and the resulting propeller wake velocity, which must be accounted for in the noise modeling.

B. Noise Characteristics of STOL Flight Procedures

In addition to noise characteristics at the source level, assessment of the noise impacts of DP, blown-flap STOL vehicles requires consideration of the flight procedures these aircraft are capable of performing. Not limited to only vehicles utilizing DP, blown-flap technology, STOL aircraft in general are capable of performing flight procedures that may result in unique noise signatures at the community level compared to conventional take off and landing (CTOL) aircraft. Per their namesake, STOL vehicles, such as the Helio Courier aircraft and the MIT sub-scale demonstrator, have the ability to perform short takeoff and landing field lengths, allowing the aircraft to climb to higher altitudes in a shorter track distance from brake release. In addition, vehicles such as the MIT demonstrator have been shown to be capable of achieving high lift coefficients (greater than 10 [6]), enabling slow flight and steep descents on arrival. Steep flight procedures have been demonstrated for commercial aircraft to reduce community noise levels when compared to conventional procedures [3]. However, the performance parameters required to achieve certain flight procedures for a given configuration must be assessed to determine the potential overall noise reduction.

III. Community Noise Modeling Methodology for DP Blown-Flap STOL Flight Procedures

The acoustic analysis methodology for DP, blown-flap STOL vehicles utilizes a noise component-based modeling approach to estimate the relevant noise sources based on flight performance requirements, and is summarized in Fig. 3. The initial input to the methodology is a segment-by-segment flight operation definition, such as a short takeoff followed by a steep climb during departure. This definition is given along with aircraft settings such as configuration

and throttle. Within the STOL flight profile model, the flight profile (such as the flight path angle and velocity) is determined, as constrained by performance parameters of the vehicle to achieve this operation, which are outputs from the STOL performance model, such as weight, drag, and available thrust. The flight profile, airframe geometry, and engine performance parameters become inputs to the noise model. As such, the modeling method evaluates the component noise levels for varying airframe or propulsor geometries, flight trajectories, and performance at different operational settings.

The framework uses methods from the NASA Aircraft Noise Prediction Program (ANOPP2) [10]. ANOPP2 incorporates both ANOPP methods to model the noise levels from various airframe and engine components at a user-defined 3-dimensional observer grid for an arbitrary flight procedure. A similar model to the one shown in Fig. 3 utilizing ANOPP modules has already been developed by the authors to evaluate the noise impact of advanced operational procedures to mitigate noise impact around airports [2, 3]. An additional example framework for electric Vertical Takeoff and Landing (eVTOL) multirotor urban air mobility vehicles is being developed by NASA [11]. The details of each model within the community noise modeling methodology are described in the following sections.

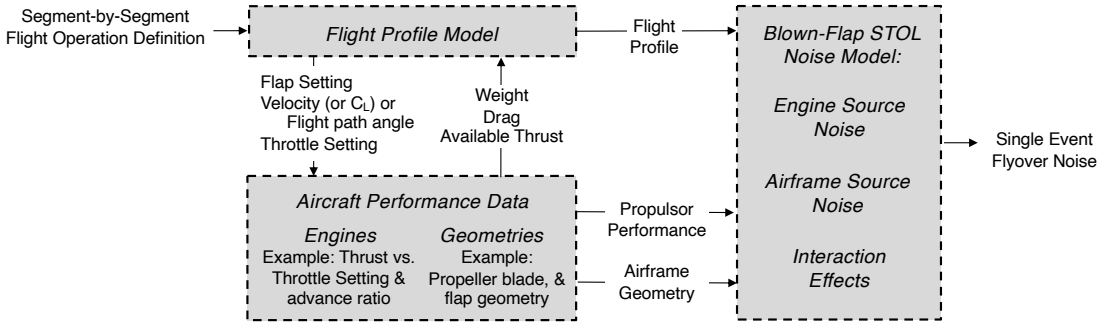

Fig. 3 Integrated flight procedure, performance, and noise modeling method to determine community noise for blown-flap STOL aircraft

A. DP Blown-flap STOL Vehicle Component Noise Modeling

The methodologies for modeling each engine, airframe, and propulsor-airframe interaction noise source for DP, blown-flap STOL vehicles, broken down in Fig. 4, are as follows. As discussed in section II.A, it is assumed that the primary noise generating engine and airframe components are the tonal and broadband components of the distributed propellers, the wing and tail trailing edge, high-lift devices, and landing gear. Additional propulsor-airframe interaction effects are also assumed, which include the interaction between the propeller wake and flap side edges, as well as the interaction between the wing trailing edge and propeller wake.

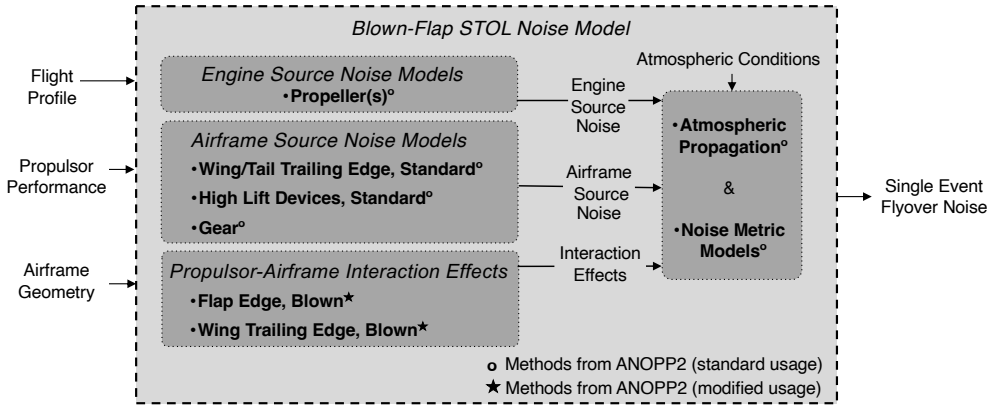

Fig. 4 Modeling methodology for blown-flap STOL aircraft component noise

Multiple propeller discrete tonal and broadband noise is modeled using ANOPP2's Blade Element Acoustic Tool (ABEAT) [12]. This method employs blade-element-momentum theory to model the rotor blade loads as lifting lines. Rotor discrete loading and thickness noise is modeled from blade shape and aerodynamic loads using Farassat methods. Propeller blade broadband self-noise is modeled from semi-empirical methods [13]. The propeller noise modeling requires the geometry of the propeller distribution with respect to the vehicle, the engine RPM and blade geometry distribution, and the vehicle forward velocity.

Airframe noise components such as the wing and tail trailing edge boundary layer interaction noise in standard, un-blown operations, are modeled using the method by Fink [8], whereas landing gear and high-lift devices such as flap edge noise in standard, un-blown operations, are modeled with the Guo methods [7, 14] implemented in ANOPP. These airframe noise methods require airframe geometry and flow velocity at each component. In particular, the Fink method assumes that the wing trailing edge noise is due to the convection of the turbulent boundary layer past the trailing edges and scales with the 5^{th} power of the flow velocity [8]. The Guo method assumes flap noise is attributed to vortex interactions at the side edge corners downstream of the flap leading edge and vortex/edge interactions in the latter half of the flap chord, which have been shown to vary with the 5^{th} and 6^{th} power of the flow velocity, respectively [7].

Additional propulsor-airframe interaction effects are estimated through modified usage of the airframe noise modules. As mentioned in section II.A, additional noise at the flap and wing trailing edge is assumed to be impacted due to the increased local flow velocity from the propeller wake compared to aircraft without distributed blown-lift. To include this effect, the propeller wake-flap and propeller wake-trailing edge interaction noise is approximated using the Guo flap side edge noise and Fink trailing edge noise models, incorporating the estimated propeller wake velocity in different operations. The estimation of the velocity of the propeller wake is described further in section III.B.

Finally, given the engine, airframe, and interaction noise sources, propagation and noise attenuation to the observers are determined from atmospheric conditions to yield single event flyover noise, which is the final output and can be represented in a variety of noise metrics such as Overall A-weighted sound pressure level (OASPL) and Sound Exposure Level (SEL).

B. DP Blown-flap STOL Vehicle Geometry, Performance, and Flight Profiles

Introduced in section III.A, the noise modeling requires detailed performance states and geometries. For propulsor noise, this includes the propeller blade cross-section airfoil shape, angle and chord per radial station, incoming velocity V_∞, and propeller rotation rate (RPM). Airframe noise components, including flaps, trailing edge and landing gear, requires the cross-section geometry, deflection angle δ_f (in the case of extendable high lift devices), and local flow velocity. For the analysis of an existing vehicle, this geometric information must be measured directly.

For most general aviation and commercial aircraft, the flow at the flap is equal to the velocity of the airplane. However, in blown-flap STOL design, it is expected that the wake caused by the propellers influences the local flow velocity at the flap. For a given propeller and operating condition, actuator disk theory is used to estimate the propeller wake velocity V_J first shown in Fig. 2 given the propeller radius R, V_{inf}, the atmospheric density ρ, and the propeller thrust T, as shown in equation 1. Required propeller thrust for a given flight condition is governed by the drag, weight, and flight path angle of the vehicle along with the desired lift coefficient for the operation. For a given propeller and motor combination, the available thrust is correlated to RPM and forward flight velocity from performance maps.

$$\left(\frac{V_J}{V_\infty}\right)^2 = \frac{T}{(\pi R^2)V^2\frac{\rho}{2}} + 1 \tag{1}$$

The high momentum jet of the propeller wake from the blown wing allows the aircraft to achieve unique performance characteristics [15]. Such high exhaust velocity increases the net effective camber of the wing, resulting in higher C_L values, as referenced in [6]. However, along with parasitic drag, the blowing effects induce higher drag due to higher lift [15]. Flow parameters of the momentum theory model of jet contraction, as referenced in [15], are used to compute the coefficient of drag due to blowing.

A point mass model and the governing equations of motion are used to obtain the flight path angle for each phase of flight, as a function of the propeller throttle setting, the number of motors operating, and the flap setting for a particular configuration. The velocity of the jet per engine is computed with equation 1 for the aerodynamics during departure (including the takeoff roll and climb), cruise, and approach (including the descent and landing roll).

STOL departure and approach flight physics indicate various characteristics that may impact overall noise levels. For example, during the climb segment of departure, there is a generally inversely proportional trend between the C_L and

climb angle due to the trade off between blowing high-lift capabilities and increased induced drag. Therefore, higher lift values produce a shallow climb angle, while lower C_L values create a steeper climb angle. Moreover, the opposite trend is observed for descent angles on approach. The descent angle increases as higher C_L values are achieved. Therefore, higher C_L values produce a steeper descent, while lower C_L values create a shallower approach angle. Finally, as already mentioned in section II.B, shorter landing and takeoff segments result from the higher lift C_L combination of shallow climb and steeper approach angles. STOL aerodynamic and performance characteristics and runway requirements unique to this vehicle are used to examine the noise levels of this vehicle in the following sections.

IV. Noise Measurement and Modeling Demonstration of DP Blown-Flap STOL Aircraft Flight Procedures

The purpose of this section is to examine the noise characteristics of representative STOL vehicle flight procedures and to demonstrate the DP Blown-Flap STOL Aircraft modeling method. Preliminary validation of the propeller noise module introduced in section III.A is presented, along with a flight test and noise measurement demonstration of STOL flight procedures versus CTOL flight procedures. Finally, the full modeling methodology presented in section III is utilized to analyse the component and flight procedural noise levels of an example DP Blown-Flap STOL vehicle.

A. Static Propeller Noise Modeling Validation

In order to validate the propeller modeling method described in III.A, the noise levels of a propeller with known geometry and operating conditions were measured and the experimental data was compared to the modeled results. The acoustic experiment consisted of a single, static 5-bladed propeller, operated in three different RPM's with a difference of 1000 RPM between each discrete case. At each RPM the A-weighted sound pressure level was recorded using 9 microphones (model SRTW-mk3 from Convergence Instruments) mounted at the propeller hub height. The microphones were spaced radially to form a half circle about the propeller shaft, as diagrammed in a top view in Fig. 5. This orientation was intended to record the variations of rotor noise moving from forward to aft locations. This setup was then used to record the noise of the isolated motor using the same discrete RPM levels.

The noise levels of this propeller were then modeled using the framework described in Fig. 4 at the same RPMs, operating conditions and position as the microphones in the experimental run. Assuming a hard ground, the isolated motor noise and ground reflections corrections were added to the modeled output, in order to compare these results with the experimental data.

The noise model results with motor noise and ground effects added are shown as continuous curves in Fig. 5 and the measured noise levels are for each RPM and microphone location as discrete points. Close correspondence in noise level was found towards the forward and aft positions of the propeller across all operating RPMs, with results agreeing to within 1 dB. Lower RPMs matched very closely across all microphone stations while higher RPMs cases diverged slightly on the sides of the rotor. The larger discrepancies around the 90-degree positions were likely explained by noise reflections and other interactions with a hard barrier that was placed for safety in the propeller plane during experimental runs. Other possible explanations for the disagreement in noise were additional reflections from the hard ground below the rotor. Otherwise, the results indicated enough congruence for initial validation of the propeller modeling method.

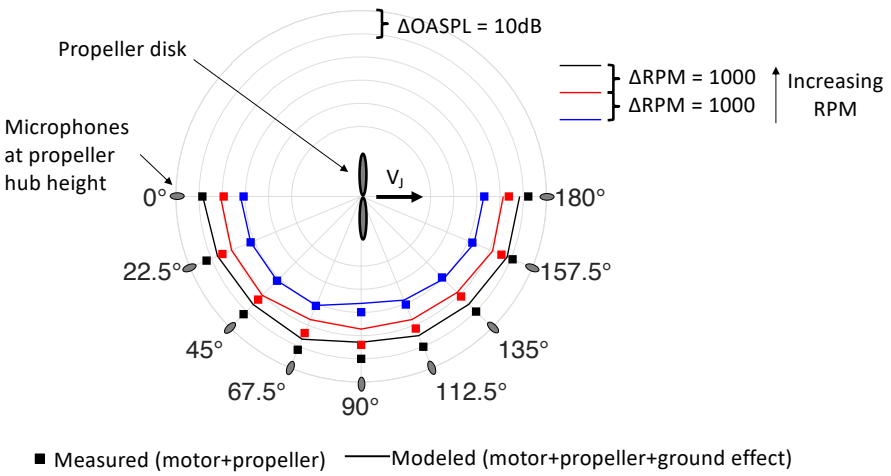

Fig. 5 Example measured and modeled static 5-bladed propeller noise levels at varied RPM settings

B. STOL Flight Procedure Test Demonstration and Measured Noise Levels

The short takeoff and landing capabilities and ability to fly steeply of STOL vehicles is assumed to have the potential for lower under-track noise levels than conventional procedures, as mentioned in section II.B. As a proof of this concept, noise measurements were taken during a flight test demonstration of an available Helio Courier aircraft. The Helio Courier is a single propeller piston engine aircraft capable of STOL departure and approach procedures and steep climb and descent profiles [16]. An aerial view of the test set up and flight procedures is presented in Fig.6. The test setup included 5 wireless sound level meters (SRTW-mk3 Convergence Instruments microphones) distributed along the runway. The maximum A-weighted sound pressure level $L_{A,Max}$ of the aircraft was recorded by the microphone, while an on board global positioning system (GPS) receiver recorded the latitude, longitude, and altitude. The sound levels were obtained from microphones 3, 4, and 5 for departures, while microphones 1, 2, and 3 were used for approaches. The experimental flight tests consisted of two STOL departures (labeled departure 1 and 2) and two STOL landings with steep descents (labeled approach 1 and 2), as well as a long takeoff roll flight (departure 3) and long landing roll flight (approach 3). The lateral positions of these flights are plotted on Fig. 6.

(a) Departure Procedures **(b) Approach Procedures**

Fig. 6 Helio aircraft STOL and long roll procedure demonstration, flight procedures and microphone arrangement

Fig. 7 shows the GPS altitude versus distance from brake release and the measured noise levels (shown as points on the right figures) for the departure procedures, while Fig. 8a shows similar results for the approach procedures. The inverse square law was used to estimate the flyover noise for the ground track beyond microphone 5 for departure, and prior to microphone 1 for approach. As expected, STOL procedures were capable of achieving an altitude of 1000ft in a shorter distance from brake release than the long takeoff roll procedure, as shown in Fig. 7a (a). Likewise, as depicted in Fig.8a when performing the STOL procedures the aircraft was capable of descending at a steeper slope than in the long roll takeoff procedure.

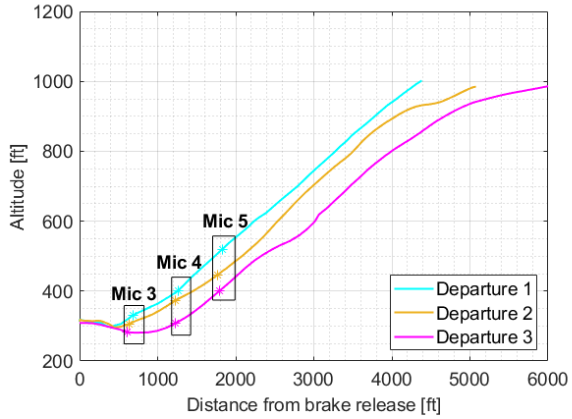

(a) GPS altitude above sea level versus distance from brake release

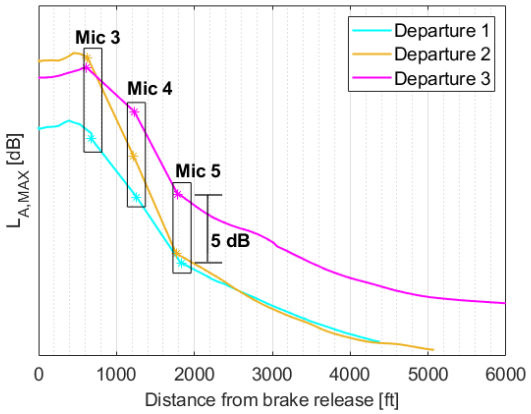

(b) Noise levels where * indicate measured data and solid lines indicate estimated noise due to spherical spreading

Fig. 7 Helio aircraft altitude and noise levels for various departure procedures

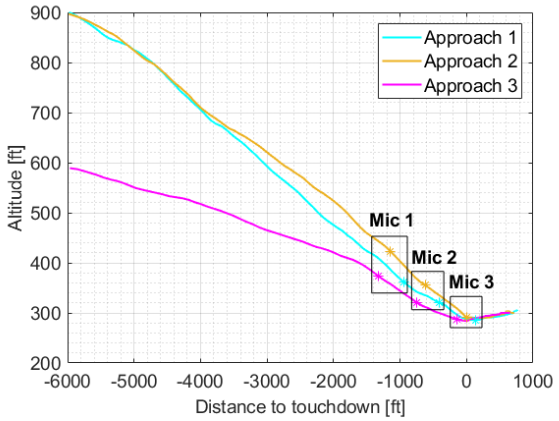

(a) GPS altitude above sea level versus distance to touchdown

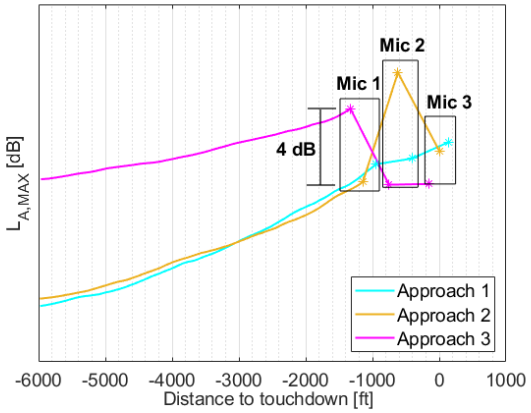

(b) Noise levels where * indicate measured data and solid lines indicate estimated noise due to spherical spreading

Fig. 8 Helio aircraft altitude and noise levels for various approach procedures

Lower noise levels for the STOL procedures seen in Fig.7b (about 5 dBA over microphone 5) and Fig.8b (about 4 dBA over microphone 1), were observed for most of the flight procedures, with the exception of a noise spike seen in the STOL 2 approach over microphone 2, observed in Fig.8b. This is presumed to be an effect of a non-precision approach and RPM variations during that procedure. The lowered noise levels were assumed to be primarily due to the altitude difference resulting from the STOL performance characteristics. These results motivate the study of the STOL flight procedures obtained through blown flaps studied in the next section.

C. Modeled Source Noise Variation of DP, Blown-Flap STOL Aircraft in Departure, Cruise, and Approach Flight Phases

To demonstrate the component-based noise modeling methodology for STOL flight procedures presented in section III, a preliminary assessment of the MIT sub-scale STOL vehicle equipped with eight 7x6" Aeronaut folding propellers from [6] is presented. The MIT sub-scale vehicle was chosen for the assessment due to its available flap geometry, propellers, and flight performance characteristics [6]. The preliminary analysis focused on a representative departure, cruise, and approach procedure, shown conceptually in Fig. 9, with the contribution of each noise source to the total noise assessed. Resulting noise levels were obtained by measuring the propeller blade and airframe geometry. Such measurements were used as inputs to the component based noise model along the flight performance characteristics.

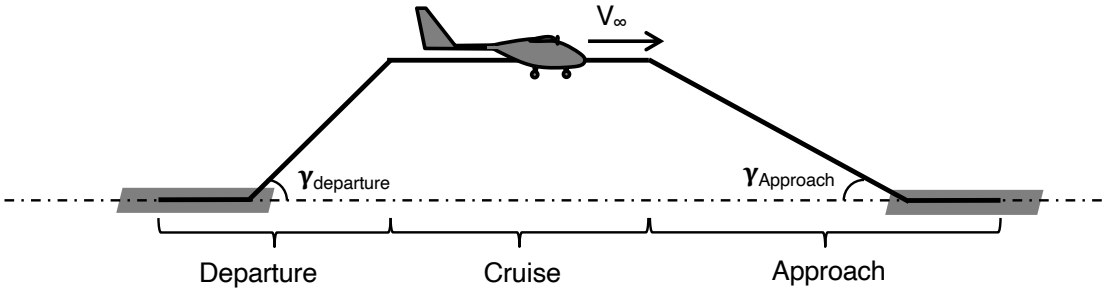

Fig. 9 Baseline departure, cruise, and approach procedure representation for DP, blown flap vehicle noise modeling

The propeller throttle setting, flight velocity, flight path angle (γ), and flap angle for each operating condition is shown in Table 1. The departure procedure conditions were achieved assuming full throttle and a flight path angle of 28° was maintained during the climb phase. Table 1 indicates the flight speed and flap setting needed to maintain this condition during climb. Such condition was based on estimated drag as described in section III.B. In addition, the available thrust was estimated from propeller performance maps for the MIT demonstrator propeller and motor combination. Similarly, Table 1 describes the resulting flight speeds and flap settings obtained for a steady cruise and continuous descent approach procedure. For the cruise and approach procedure, it was assumed that only the inner six propellers were operating as described in [6].

Table 1 Baseline operating conditions for sub-scale DP, blown flap vehicle noise modeling

Operation	Throttle Setting	Flight Speed V_∞ (knots)	Flight Path Angle γ (°)	Flap Setting δ_f (°)
Departure	Full	18	28	25
Cruise	Full	63	0	0
Approach	50%	12	-8.9	40

As mentioned in section III.A, propeller noise modeling requires detailed propeller blade geometry and performance information. This includes the blade airfoil coordinates, resulting lift and drag coefficients, blade radius and number, and propeller RPM. The throttle setting and forward flight speed was mapped to an RPM and thrust for each propeller. This data was used in the modeling method to estimate the tonal loading and thickness noise for each propeller. Equation 1 was used to determine the propeller wake velocity V_J for each condition. The wake velocity and flap geometry were used to estimate the propeller wake-flap interaction noise using the Guo flap method[7], as mentioned in section III.A, assuming the wake velocity to be the local velocity at the flap edges. In addition, the wake velocity along with the wing geometry was used to estimate the propeller wake-wing trailing edge interaction noise using the Fink method[8] as mentioned in section III.A, assuming the wake velocity to be the local velocity at the wing trailing edge.

A-weighted maximum sound pressure level $L_{A,Max}$ noise from the modeling method described in section III, is shown for the combined propeller noise and the combined airframe noise components in Fig. 10. Such results are

obtained based on the operating conditions shown in Fig. 1 and Table 1. Each case seen in Fig. 10 is the modeled noise for an observer located 50 feet directly underneath the vehicle.

The analysis indicates that the relative magnitude of each noise source compared to each other is dependent on the operating condition. The propeller noise dominates at nearly all phases, while the relative contribution of the airframe noise depends strongly on the phase of flight. For example, the total propeller noise levels in departure is shown to be over 10 dBA louder than the total airframe noise. During the approach, the airframe noise, which was primarily dominated by propeller wake-flap interaction noise, becomes closer in magnitude to the total propeller noise, although the noise levels are overall lower compared to the takeoff case. Higher air speeds during the cruise phase resulted in higher propeller noise levels than in departure, though airframe noise compared to propeller noise is small due to the aircraft having flaps retracted in this configuration.

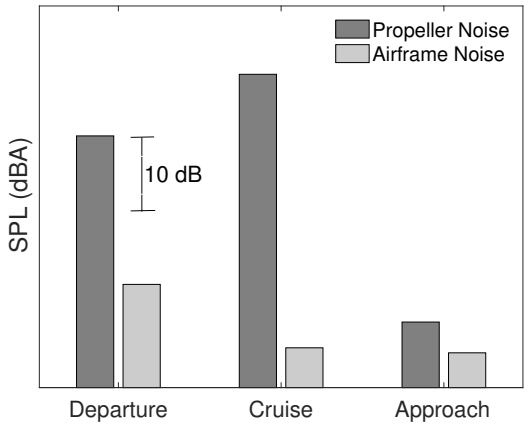

Fig. 10 Modeled propeller and airframe noise levels of sub-scale STOL demonstrator at 50 feet overhead for different operating conditions, $L_{A,Max}$ (dB)

In addition to the overflight noise levels, the single event noise contours for the full departure and approach procedures were also modeled. Fig. 11 shows the component and total sound exposure level (SEL) noise contours at low, medium, and high decibel levels during the STOL departure procedure. At all decibel levels for departure, the total noise, plotted as solid lines, was dominated primarily by propeller noise, shown as dashed lines. This is especially apparent in the low dB contour level (shown in black), where the airframe noise, represented by dotted lines, occupies less than 5 percent of the area of both the total and propeller noise.

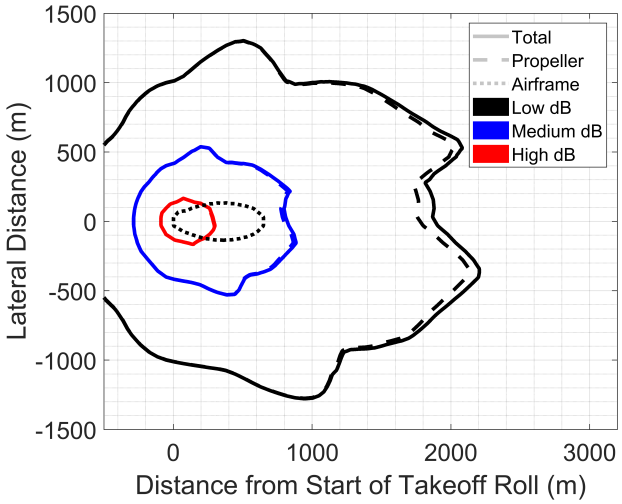

Fig. 11 Modeled propeller and airframe noise contours of sub-scale STOL demonstrator in a 28° climb during departure, SEL levels each separated by 10 dB

The approach case in Fig. 12, which shows the modeled low, medium, and high decibel SEL contour levels for the approach procedure from Fig. 1, differs from the departure case. In the approach case, the airframe noise, shown in dotted lines, accounts for a larger fraction of the total noise. At the low decibel level on approach, the airframe makes up a substantial, 30 percent of the total noise. Still, even in this operating condition, the propeller noise results in contours of greater area than the airframe at all levels and accounts for the majority of the noise especially at the medium and high decibel levels. The approach case also has noticeably smaller and narrower contours than the departure case. At medium decibel levels, the approach contour is just over 1000 m long and 200 m wide whereas the takeoff contour is about 2500 m long and 2200 m wide. These results indicate that in both takeoff and approach flight procedures, propeller noise is the main noise source for a DP, blown-flap STOL aircraft. Although not the primary contributor for total noise, the results do indicate that airframe noise has the potential to be a relevant noise source during landing.

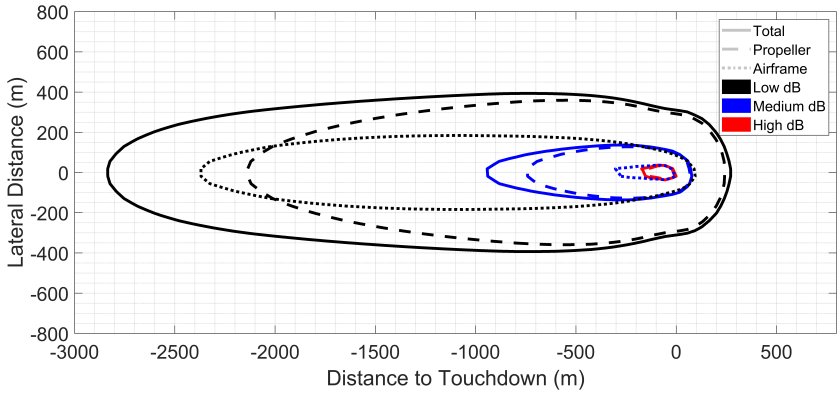

Fig. 12 Modeled propeller and airframe noise contours of sub-scale STOL demonstrator in a -8.9° landing, SEL each separated by 10 dB

D. Demonstration of Analysis of the Overflight Noise for DP, Blown-Flap STOL Aircraft Performing Varied Approach Procedures

Various flight path angles can be achieved for both departure and approach operations with different combinations of propeller throttle settings and flight velocities. In turn, resulting noise levels will also vary. To demonstrate this, the analysis of the total noise variation for the sub-scale DP, blown-flap STOL aircraft from section IV.C is presented during different approach procedures.

As conceptually diagrammed in Fig. 13, various glide angles can be adopted during approach that vary the distance and time spent over a certain ground area. This can be achieved through adjustments in flight speed and throttle setting for a certain descent angle and landing field length. The performance and acoustic footprints of these various approach procedures can be analyzed and used to assess potential noise abatement for DP blown-flap STOL vehicles.

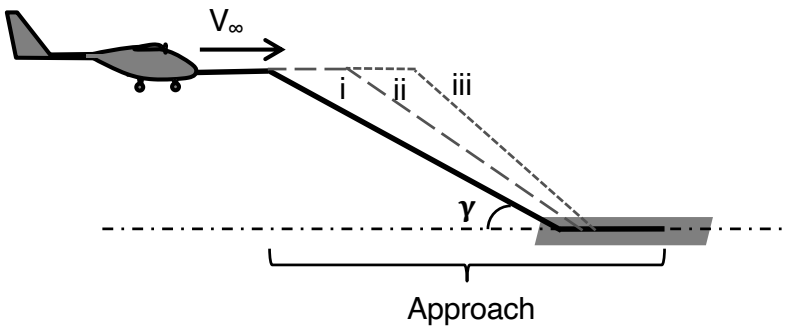

Fig. 13 Representation of alternate approach procedures for DP, blown flap vehicle noise modeling

Table 2 describes the approach procedures considered for the presented analysis. They included one set of high-powered (50%) approach throttle cases and one set of low powered (25%) approach throttle cases. For each throttle setting, three different flight path angles and corresponding approach velocities were modeled to create three cases of increasingly steeper approach.

Table 2 Approach procedure operating conditions for sub-scale STOL noise modeling

Operation	Case	Throttle Setting	Flight Speed V_∞ (knots)	Flight Path Angle γ (°)	Flap Setting δ_f (°)
High Power	i	50%	17	-3.1	40
Approach	ii	50%	12	-8.9	40
	iii	50%	10	-15.6	40
Low Power	i	25%	17	-6.9	40
Approach	ii	25%	12	-11.5	40
	iii	25%	10	-16.9	40

The noise levels of the aircraft were modeled for each of the procedures from table 2. Fig. 14 shows modeled SEL low and high decibel levels for the high-powered approaches at three different glide slopes with slope III the steepest, shown in solid lines. The low and high levels are each separated by 20 dB. The contours become narrower and longer as the glide slope decreases. This is especially clear in the high decibel case, where Path III forms a curve 1500 m long, and 900 m wide where the shallower Path I forms a longer and skinnier curve 2500 m long and 200 m wide. Changes in slope have a stronger correlation to changing shape, rather than total area.

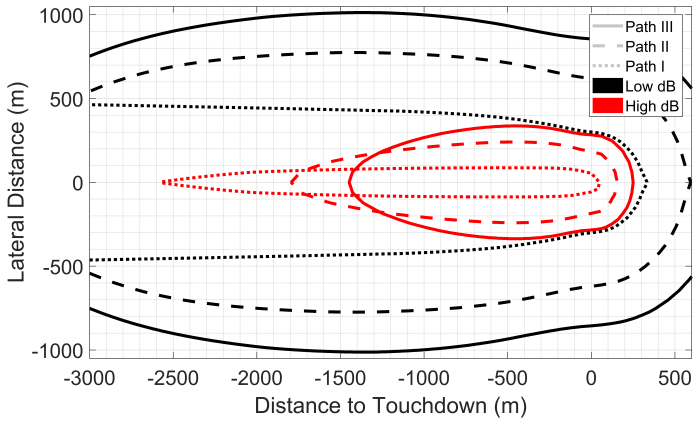

Fig. 14 Modeled high-power approach noise contours of sub-scale STOL demonstrator, SEL levels each separated by 20 dB

This pattern, however, is less apparent in the low-powered approaches shown in Fig. 15. Steeper glide slopes form ellipses of consistently smaller area than that of shallower slopes. At the low decibel level, Path III forms a curve 500 m long and 200 m wide, where the shallower Path I forms a curve 1500 m long and 800 m wide. Compared to the high-powered case the low-powered approach creates contours greatly smaller at all glide slopes. At low decibels, the low-powered contour is just over 250 m in length, where the high-powered case creates curves of over 2000 m in length. The largest change in total noise was achieved when adjusting the aircraft throttle during approach. Within each power setting, however, the results indicate a wide amount of different noise profile exist when flight path angle is adjusted, with certain angles causing a decisive reduction of total noise.

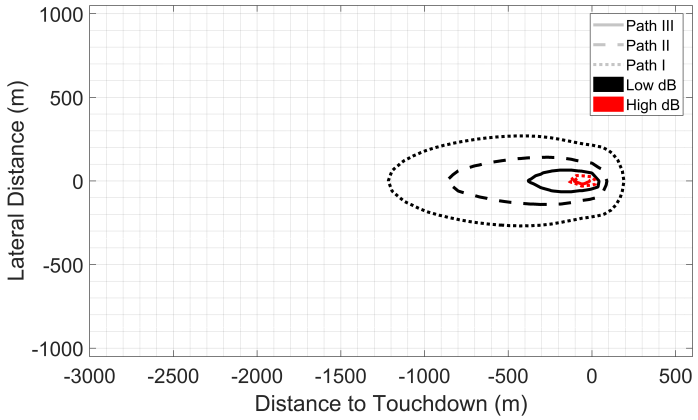

Fig. 15 Modeled low-power approach noise contours of sub-scale STOL demonstrator, SEL levels each separated by 20 dB

V. Conclusion

As advanced air mobility is gaining popularity, short takeoff and landing vehicles, equipped with unconventional high-lift devices, are being proposed throughout the industry. The ability to achieve higher lift coefficients is favorable for performing short takeoffs and landings. However, the noise levels necessary to achieve these flight characteristics must be assessed along with the flight performance to total noise level sources. In this work, the overflight noise variation of conventional and short takeoff and landing procedures was measured in a Helio Courier flight test. The results obtained show how STOL aircraft can perform procedures with steeper climb and descent angles than conventional ones. The test data suggests that the ability to reach a given altitude in a shorter distance results in a lower observer noise.

In addition, a methodology that models and evaluates the source component noise levels was developed to analyze the noise contributions and trade-offs of STOL vehicle characteristics, including those which can be achieved with distributed propulsion and blown flaps. The local flow velocity is increased at aerodynamic surfaces such as the flaps and wing trailing edge for DP blown-flap vehicles, resulting in propeller wake-aerodynamic surface interaction noise. Propeller arrangement, RPM, aircraft speed, and flap deflection are used to predict and study the noise characteristics using the presented noise model.

Initial component-based noise modeling shows that the magnitude of noise for each sub-component varies heavily and depends on the operating conditions. The majority of the noise was found to be caused by the propellers based on modeled results. However, the results indicate that the airframe may potentially be a major contributor to the total noise, though this should be confirmed with future validation efforts. When the effects of approach procedure variation were modeled, the results indicated that aircraft power and flight approach angle had a large influence on both the shape and magnitude of noise. These conclusions indicate that a large degree of noise attenuation and control is possible due to the wide operating condition capabilities of STOL aircraft.

References

[1] Rizzi, S. A., and et. al., "Urban Air Mobility Noise: Current Practice, Gaps, and Recommendations," NASA TP–2020-5007433, 2020.

[2] Thomas, J., Mahseredjian, A., Salgueiro, S., and Hansman, R. J., "Delayed Deceleration Approach Procedure Noise Modeling Validation using Noise Measurements and Radar Data," *AIAA Aviation 2021 Forum*, 2021. https://doi.org/10.2514/6.2021-2135.

[3] Thomas, J., and Hansman, R. J., "Framework for Analyzing Aircraft Community Noise Impacts of Advanced Operational Flight Procedures," *Journal of Aircraft*, Vol. 54, No. 4, 2019. https://doi.org/10.2514/1.C035100.

[4] Courtin, C., Mahseredjian, A., Dewald, A. J., and Hansman, R. J., "A Performance Comparison of eSTOL and eVTOL Aircraft," *AIAA AVIATION 2021 FORUM*, 2021. https://doi.org/10.2514/6.2021-3220.

[5] Agrawal, D., and *et al*, "Wind Tunnel Testing of a Blown Flap Wing," AIAA 2019-3170, AIAA Aviation, 2019.

[6] Courtin, C., Hansman, R. J., and Drela, M., "Flight Test Results of a Subscale Super-STOL Aircraft," AIAA 2020-0977, AIAA Scitech 2020 Forum, 2020.

[7] Guo, Y., "Aircraft Flap Side Edge Noise Modeling and Prediction," 32nd AIAA Aeroacoustics Conference, 2011.

[8] Fink, M., "Airframe Noise Prediction Method," Tech. Rep. FAA-FRD-77-29, 1977.

[9] Reddy, N. N., "Blown Flap Noise Prediction," Tech. Rep. NASA-CR-158978, Hampton, Virginia, 1978.

[10] Lopes, L. V., and Burley, C. L., "ANOPP2 User's Manual: Version 1.2," NASA TM 2016-219342, 2016.

[11] Krishnamurthy, S., Rizzi, S., and *et al*, "Prediction-Based Auralization of a Multirotor Urban Air Mobility Vehicle," *AIAA Scitech 2021 Forum*, 2021. https://doi.org/10.2514/6.2021-0587.

[12] Krishnamurthy, S., Tuttle, B. C., and Rizzi, S., "A Synthesis Plug-in for Steady and Unsteady Loading and Thickness Noise Auralization," AIAA AVIATION 2020 FORUM, 2020.

[13] Brooks, T. F., Pope, D. S., and Marcolini, M. A., "Airfoil Self-Noise and Prediction," Tech. Rep. NASA-RP-1218, Hampton, Virginia, 1989.

[14] Guo, Y., "An Improved Landing Gear Noise Prediction Scheme," Tech. Rep. NASA/CR-NAS1-NNL04AA11B, The Boeing Company, Huntington Beach, CA, 2006.

[15] Courtin, C., "An Assessment of Electric STOL Aircraft, Master's Thesis," *Massachusetts Institute of Technology*, 2019.

[16] Rowe, F. J., *The Helio Courier Ultra C/STOL aircraft*, Jefferson, NC. McFarland & Company, Inc., 2006.